Singlet-quintet mixing in spin-orbit coupled superconductors with j=3/2 fermions

Jiabin Yu and Chao-Xing Liu

Phys. Rev. B **98**, 104514 — Published 27 September 2018

DOI: 10.1103/PhysRevB.98.104514

Singlet-Quintet Mixing in Spin-Orbit Coupled Superconductors with $j = 3/2$ Fermions

Jiabin Yu[1] and Chao-Xing Liu[1,*]

[1] *Department of Physics, the Pennsylvania State University, University Park, PA, 16802*

In non-centrosymmetric superconductors, spin-orbit coupling can induce an unconventional superconducting state with a mixture of s-wave spin-singlet and p-wave spin-triplet channels. It is commonly thought that inversion symmetry breaking is substantial for pairing-mixed superconducting states. In this work, we theoretically propose that a new type of pairing-mixed state, namely the mixture of s-wave spin-singlet and d-wave spin-quintet channels, can occur even in the presence of inversion symmetry when electrons effectively carry "spin-3/2". As a physical consequence of the singlet-quintet pairing mixing, topological nodal-line superconductivity is found in such system and gives rise to flat surface Majorana bands. Our work provides a possible explanation of unconventional superconducting behaviors observed in superconducting half-Heusler compounds and suggests that these superconducting materials provide a new platform for exploring unconventional and topological superconductivity.

I. Introduction

In conventional Bardeen-Cooper-Schrieffer theory of superconductivity, the simple s-wave spin-singlet pairing relies on the presence of time reversal (TR) and inversion symmetry (IS) in superconductor (SC) materials. In non-centrosymmetric SCs, it has been recognized that the IS breaking can give rise to superconducting states with mixed pairing, namely p-wave spin-triplet component mixed into s-wave spin-singlet pairing[1–3]. Such type of mixed pairing superconductivity has been demonstrated experimentally in various non-centrosymmetric SCs, e.g. Ce-based heavy fermion SCs[1], and can lead to a variety of exotic phenomena, including anisotropic upper critical field[1,4–7], magnetoelectric effect[1,8–10], topological superconductivity[11–13], *et al*[1].

Recently, increasing research attention has been focused on non-centrosymmetric superconducting half-Heusler compounds[14], owing to the "spin-3/2" nature of electrons in the low energy sector. Here "spin" refers to the total angular momentum j, which is a combination of 1/2-spin and angular momentum of p atomic orbitals ($l = 1$), of basis electronic states. In contrast to spin-1/2 SCs with only singlet and triplet states, the Cooper pairs of $j = 3/2$ electrons can carry total spin $S = 0$ (singlet), 1 (triplet), 2 (quintet) and 3 (septet). As a result, a variety of pairing forms have been theoretically considered, including mixed singlet-septet pairing[14–17], s-wave quintet pairing[14,17–19], d-wave quintet pairing[20,21], odd-parity (triplet and septet) parings[20–23], *et al*[21]. Recent experiments have also revealed unconventional superconducting properties[15,24–26]. In particular, the power-law temperature dependence of London penetration depth observed in Ref.[15] indicates the existence of nodal lines in half-Heusler SCs and is interpreted as the consequence of the mixing between dominant p-wave septet and subdominant s-wave singlet channels. Inversion-asymmetric spin-orbit coupling (SOC) due to the absence of IS in the crystal of half-Heusler compounds is expected to play an essential role in inducing such pairing mixing. In this work, we point out that the centrosymmetric part of the SOC is more important for understanding superconducting properties in half-Heusler SCs. We demonstrate that the centrosymmetric Luttinger SOC can induce the mixing between s-wave spin-singlet and isotropic d-wave spin-quintet channels and lead to topological nodal-line superconductivity (TNLS). Therefore, our results provide an alternative explanation of the temperature dependence of London penetration depth. Furthermore, our work provides the *first* concrete microscopic mechanism for pairing mixing between two spin channels in the inversion-preserving class (IS is allowed to exist), whereas all previous works on pairing mixing require IS breaking. Therefore, it is expected that the singlet-quintet mixing mechanism can also be applied to centrosymmetric SCs with high-spin electrons, such as Sr_3SnO[27–30], as well as cold atom systems[31].

II. Model Hamiltonian

We start from band structures of half-Heusler compounds and illustrate the origin of $j = 3/2$ electrons. The energy bands near the Fermi energy in half-Heusler compounds are s-orbital-like bands (Γ_6 bands) and p-orbital-like bands, where the latter is split into $j = 3/2$ bands (Γ_8 bands) and $j = 1/2$ bands (Γ_7 bands) by SOC[32]. For half-Heusler SCs with p-type carriers like YPtBi[24], only the Γ_8 bands are relevant[33]. The bases of Γ_8 bands can be labeled as $|j, j_z\rangle$, where $j = 3/2$ is the total angular momentum that can be effectively regarded as "spin" and $j_z = 3/2, 1/2, -1/2, -3/2$. The low energy physics of the Γ_8 bands is described by the so-called Luttinger model[33,34] with the Hamiltonian

$$h(\mathbf{k}) = \xi_{\mathbf{k}}\Gamma^0 + h_{SOC}(\mathbf{k}) = \xi_{\mathbf{k}}\Gamma^0 + c_1\sum_{i=1}^{3} g_{\mathbf{k},i}\Gamma^i + c_2\sum_{i=4}^{5} g_{\mathbf{k},i}\Gamma^i \tag{1}$$

where $\xi_{\mathbf{k}} = \frac{1}{2m}k^2 - \mu$ with the chemical potential μ, g_i's are d-orbital cubic harmonics, Γ^0 is the identity matrix and Γ^i's ($i = 1, \ldots, 5$) are five Γ matrices.[35] We define h_{SOC}[32,41,42] term as the symmetric SOC[34] in the con-

text of the Luttinger model for "spin-3/2" electrons since this term splits the $|\frac{3}{2},\pm\frac{3}{2}\rangle$ and $|\frac{3}{2},\pm\frac{1}{2}\rangle$ bands and preserves IS, while the antisymmetric SOC, which breaks IS and gives rise to spin splitting between the $|\frac{3}{2},+\frac{3}{2}\rangle$ ($|\frac{3}{2},+\frac{1}{2}\rangle$) and $|\frac{3}{2},-\frac{3}{2}\rangle$ ($|\frac{3}{2},-\frac{1}{2}\rangle$) bands, will be discussed at the end. The Luttinger Hamiltonian $h(\mathbf{k})$ has $O(3)$ symmetry if $c_1 = c_2$ and O_h symmetry if $c_1 \neq c_2$. The eigen-states of $h(\mathbf{k})$ are doubly degenerate with eigen-energies $\xi_\pm(\mathbf{k}) = k^2/(2m_\pm) - \mu$, where the subscript $\pm$ labels two spin-split bands, and $m_\pm = m/(1 \pm 2mQ_c)$ with $Q_c = \sqrt{c_1^2Q_1^2 + c_2^2Q_2^2}$, $Q_1 = \sqrt{\hat{g}_1^2 + \hat{g}_2^2 + \hat{g}_3^2}$, $Q_2 = \sqrt{\hat{g}_4^2 + \hat{g}_5^2}$ and $\hat{g}_i = g_i/k^2$. We focus on the parameter regime with $m < 0$[43], $\mu < 0$ (p-type carriers), and $c_1c_2 > 0$ for simplicity. With the choice of these parameters, the effective mass m_- of the ξ_- band is always negative while there are three different regimes for m_+ of the ξ_+ band: (I) $m_+ < 0$, (II) $m_+ > 0$, and (III) the sign of m_+ being angular dependent. Energy dispersions and Fermi surface shapes in these three regimes are depicted in Fig.1a. In realistic materials, the regime I appears for the normal band structure when Γ_6 bands have higher energy than Γ_8 bands while the regime II exists for the inverted band structure with Γ_6 bands below Γ_8 bands.[33] In the regime III, the ξ_+ band disperses oppositely along the directions $\Gamma - X$ and $\Gamma - L$, thus forming a saddle point at Γ (Fig.1a(iii)) and hyperbolic Fermi surface (Fig.1a(vi)). In realistic materials[26,43], the ξ_+ bands should eventually bend up at a large momentum in all directions (the dashed lines in Fig. 1a(iii) and (vi)). Thus, the Luttinger model is only valid in a small momentum region around Γ in the regime III.

Next we will discuss the interaction Hamiltonian and the possible superconducting pairings, especially those induced by symmetric SOC h_{SOC}. In analog to the singlet-triplet mixing, in which the p-wave character of triplet channel originates from the p-wave nature of antisymmetric SOC term[3], it is natural to expect that the pairing channel that is mixed into singlet channel due to h_{SOC} should have d-wave nature with orbital angular momentum $L = 2$, given the d-wave $g_{\mathbf{k},i}$ in h_{SOC}. According to the symmetry classification of the gap function for $j = 3/2$ fermions[22,35], the only channel that belongs to the same irreducible representation of $O(3)$ group as s-wave singlet channel is the isotropic d-wave quintet channel, which carries (L, S, J)=(2,2,0) with spin S=2 (quintet) and total angular momentum J=0 ($\mathbf{J} = \mathbf{L} + \mathbf{S}$) for the Cooper pair. Thus, the isotropic d-wave quintet channel is allowed to mix with s-wave singlet channel under $O(3)$ symmetry according to Ginzburg-Landau theory, which can be justified by the coupled linearized gap equations[35]. Here we focus on a minimal $O(3)$-invariant interaction

$$H_I = \frac{1}{2\mathcal{V}}\left(V_0 P_s P_s^\dagger + V_1 P_q P_q^\dagger\right) \tag{2}$$

in the s-wave singlet and d-wave quintet channels, where $P_s = \sum_{\mathbf{k}} c_{\mathbf{k}}^\dagger(\Gamma^0\gamma/2)(c_{-\mathbf{k}}^\dagger)^T$, $P_q = \sum_{\mathbf{k}} c_{\mathbf{k}}^\dagger(a^2\mathbf{g}_{\mathbf{k}} \cdot \mathbf{\Gamma}\gamma/2)(c_{-\mathbf{k}}^\dagger)^T$, and V_0 and V_1 stand for the s-wave and d-wave interaction parameters, respectively. Here $c_{\mathbf{k}}^\dagger$ is the four-component creation operator on the basis $|j, j_z\rangle$, $\gamma = -\Gamma^1\Gamma^3$ is the TR matrix, $\mathcal{V}$ is volume and a is lattice constant. The above interaction Hamiltonian H_I can be extracted from the electron-optical phonon interaction.[22,35]

III. Coupled linearized gap equation and singlet-quintet mixing

Based on the interaction form in Eq.2, we choose the gap function with the form $\Delta(\mathbf{k}) = \Delta_0(\Gamma^0\gamma/2) + \Delta_1(a^2\mathbf{g}_{\mathbf{k}} \cdot \mathbf{\Gamma}\gamma/2)$, in which Δ_0 and Δ_1 represent s-wave singlet and isotropic d-wave quintet channels, respectively. The corresponding coupled linearized gap equation can be derived as[35]

$$\begin{pmatrix} \tilde{\Delta}_0 \\ \tilde{\Delta}_1 \end{pmatrix} = x \begin{pmatrix} \frac{1}{2}\lambda_0 y_1 & \frac{1}{2}\lambda_0 y_2 \\ \frac{1}{2}\tilde{\lambda}_1 y_2 & \frac{1}{2}\tilde{\lambda}_1 y_3 \end{pmatrix} \begin{pmatrix} \tilde{\Delta}_0 \\ \tilde{\Delta}_1 \end{pmatrix}, \tag{3}$$

where $x = \ln[2e^{\bar{\gamma}}\epsilon_c/(\pi k_B T)]$, $\bar{\gamma}$ is the Euler constant, k_B is Boltzman constant, T is the critical temperature, ϵ_c is the energy cut-off for the attractive interaction($V_{0,1} < 0$), $\lambda_0 = -V_0 N_0$ and $\tilde{\lambda}_1 = -(2m\mu a^2)V_1 N_0$ are the normalized interaction parameters with the density of state N_0, and $\tilde{\Delta}_0 = \Delta_0 \mathrm{sgn}(c_1)$ and $\tilde{\Delta}_1 = \Delta_1(2m\mu a^2)$ are the normalized order parameters. The band information is included in the functions $y_{1,2,3}$. In the limit $\epsilon_c/2Q_c k_F^2 \ll 1$, $k_B T/\epsilon_c \ll 1$ and $\epsilon_c/|\mu| \ll 1$, the functions $y_{1,2,3}$ can be perturbatively expanded as $y_1 = \langle \mathrm{Re}[\tilde{m}_-^{3/2} + \tilde{m}_+^{3/2}]\rangle$, $y_2 = \langle \mathrm{Re}[-\tilde{m}_-^{5/2} + \tilde{m}_+^{5/2}]\ f_Q\rangle$ and $y_3 = \langle \mathrm{Re}[\tilde{m}_-^{7/2} + \tilde{m}_+^{7/2}]\ f_Q^2\rangle$ up to the leading order, where Re[...] means taking the real part, $\langle ... \rangle$ represents averaging over the solid angle, $f_Q = (|c_1|Q_1^2 + |c_2|Q_2^2)/Q_c$ and $\tilde{m}_\pm = m_\pm/m$ are the normalized effective masses of the $\xi_\pm$ bands. If $c_{1,2} = 0$, the off-diagonal term in the gap equation would be zero ($y_2 = 0$) due to $\tilde{m}_+ = \tilde{m}_-$, thus revealing the essential role of h_{SOC} in singlet-quintet mixing.[35]

By solving Eq.(3), the mixing ratio $\tilde{\Delta}_1/\tilde{\Delta}_0$ is evaluated numerically as a function of $|2mc_1|$ in Fig.1b (blue line) for $c_2 = 2c_1$ and $\tilde{\lambda}_1 = 0.1\lambda_0$, which reveals different behaviors in three parameter regimes I, II and III. $\tilde{\Delta}_1/\tilde{\Delta}_0$ increases rapidly with $|2mc_1|$ in regime I, and diverges in regime III. The dominant d-wave quintet pairing in regime III originates from the faster divergence of y_3 compared to $y_{1,2}$ in Eq. (3). To take into account the limitation of the Luttinger model in parameter regime III, a momentum cut-off Λ is introduced in computing $y_{1,2,3}$[35]. With Λ, a peak structure of $\tilde{\Delta}_1/\tilde{\Delta}_0$ (the red line in Fig. 1b) is found and confirms the dominant role of d-wave quintet pairing in regime III. Other features of $\tilde{\Delta}_1/\tilde{\Delta}_0$ in the regime III (e.g. the kinks) can be traced back to the behaviors of $y_{1,2,3}$ as a function of $|2mc_1|$[35]. With further increasing $|2mc_1|$ (regime II), $\tilde{\Delta}_1/\tilde{\Delta}_0$ drops rapidly due to the disappearance of Fermi surface for the ξ_+ bands and thus simple s-wave singlet pairing dominates in this regime. In Fig.1c, the critical temperatures

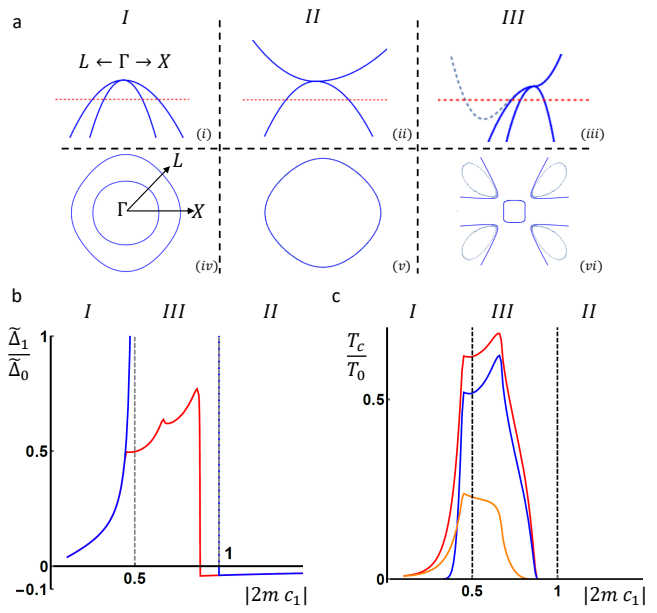

FIG. 1. (a) Energy dispersions along $X \leftarrow \Gamma \rightarrow L$ are shown in (i), (ii) and (iii) (Solid lines), and the corresponding Fermi surfaces in $X-\Gamma-L$ plane are shown in (iv), (v) and (vi) for the Luttinger model in the regime I, II and III, respectively. The dashed lines in (iii) and (vi) depict energy dispersions and Fermi surfaces for the regime III in realistic compounds. The red dashed line represents the chemical potential. The ratio $\tilde{\Delta}_1/\tilde{\Delta}_0$ and the critical temperature T_c are shown in (b) and (c) as a function of $|2mc_1|$ for $c_2 = 2c_1$, $\lambda_0 = 0.2$ $\tilde{\lambda}_1 = 0.1\lambda_0$ and $T_0 = 2e^{\bar{\gamma}}\epsilon_c/(\pi k_B)$. The blue and red lines in (b) corresponds to the case without and with momentum cut-off $\Lambda = 3\sqrt{2m\mu}$, respectively. The red line in (c) stands for the critical temperature with pairing mixing while the blue and orange lines give the critical temperatures of pure quintet and singlet channels without mixing, respectively.

T_c as a function of $|2mc_1|$ are revealed by the red line for the pairing mixing case, and by the orange and blue lines for the pure singlet and quintet cases, respectively (by neglecting the pairing mixing term in Eq. (3)). We find that (i) pairing mixing can help enhance critical temperature; and (ii) singlet pairing dominates for most of regime I and the entire regime II while quintet pairing plays a vital role around regime III.

IV. Topological nodal-line superconductivity

Similar to the singlet-triplet mixing in non-centrosymmetric SCs[1,11,44–46], a physical consequence of singlet-quintet mixing is the existence of TNLS in certain parameter regimes. The nodal line can be extracted from the Bogoliubov-de Gennes Hamiltonian with the gap function determined by the gap equation (3). We can project the gap function onto the Fermi surfaces of the $\xi_\pm$ bands, resulting in the form $\frac{\mathrm{sgn}(c_1)}{2}(\tilde{\Delta}_0 \pm \tilde{\Delta}_1 \tilde{k}^2 f_Q)$ with $\tilde{k}^2 = k^2/(2m\mu)$[35]. Consequently, the existence condition of nodal structure is determined by $\tilde{\Delta}_0 \pm \tilde{\Delta}_1 \tilde{m}_\pm f_Q = 0$. Physically, this means that the nodal structure originates from the cancellation between the singlet pairing (Δ_0 term) and the quintet pairing (Δ_1 term) and thus the singlet-quintet mixing is essential. The solutions of the above equations suggest that TNLS can exist in the regime II when $V_0 < 0$ and $V_1 > 0$ and in the regime I and III as long as $V_0 < 0$.[35] Below we focus on the regime I with normal band structure and $V_{0,1} < 0$.

Fig.2a shows the phase diagram as a function of SOC strength $|2mc_1|$ and interaction strength ratio $\tilde{\lambda}_1/\lambda_0$. Nodal rings are found in the yellow and red regions of Fig.2a for the ξ_- band (Fig. 2b and e). Due to TR and IS, a four-fold degeneracy exists at each momentum of the nodal rings. Fig. 2b (i-iv) reveals the evolution of nodal rings along the path α depicted in the inset of Fig. 2a. Six nodal rings first emerge and center around the (001), (010) and (100) axes in Fig.2b (i). These nodal rings expand (Fig.2b (ii)) and touch each other, resulting in a Lifshitz transition (Fig.2b (iii)). After the transition, eight nodal rings appear with their centers at the (111) and other three equivalent axes (Fig.2b (iv)). These eight nodal rings shrink to eight points and eventually disappear. Topological nature of these nodal rings can be extracted by evaluating topological invariant N_w of one dimensional AIII class along the loop shown by the red circle in Fig.2b(i)[35,47–49]. Direct calculation gives $N_w = \pm 2$, coinciding with four-fold degeneracy mentioned above. Non-zero N_w also implies the existence of Majorana flat bands at the surface. Fig. 2c and d show the zero-energy density of states and the energy dispersions at the (111) surface, which are calculated from the iterative Green's function method[50]. The evolution of surface Majorana flat bands follows that of nodal rings, as shown in Fig. 2c (i-iv) and d (i-iv). Additional nodal rings exist in the red region of the phase diagram (Fig. 2a), as shown in Fig. 2e, given by an extra solution of the nodal condition.

V. Discussion and Conclusion

Now we discuss the experimental implications of our theory. Previous theoretical studies on half-Heusler SCs mainly focus on the compounds in regime II (inverted band structure), while our study suggests that regimes I (normal band structure) and III (a special case of inverted band structure) are more interesting due to strong singlet-quintet mixing. Superconductivity has been found in DyPdBi and YPdBi with normal band structure[51] and critical temperatures around $0.8K$ and $1.6K$, respectively, thus providing good candidates for TNLS. YPtBi and LuPdBi are SCs with inverted band structure[33] and recent first principles calculations[14,26,43] suggest that their energy dispersion might belong to regime III, though debates still exist[14,15]. Evidence of TNLS has been found in YPtBi via the penetration depth experiment[15]. Previous studies[14,15] attribute the nodal structure to the mixing between p-wave septet pairing

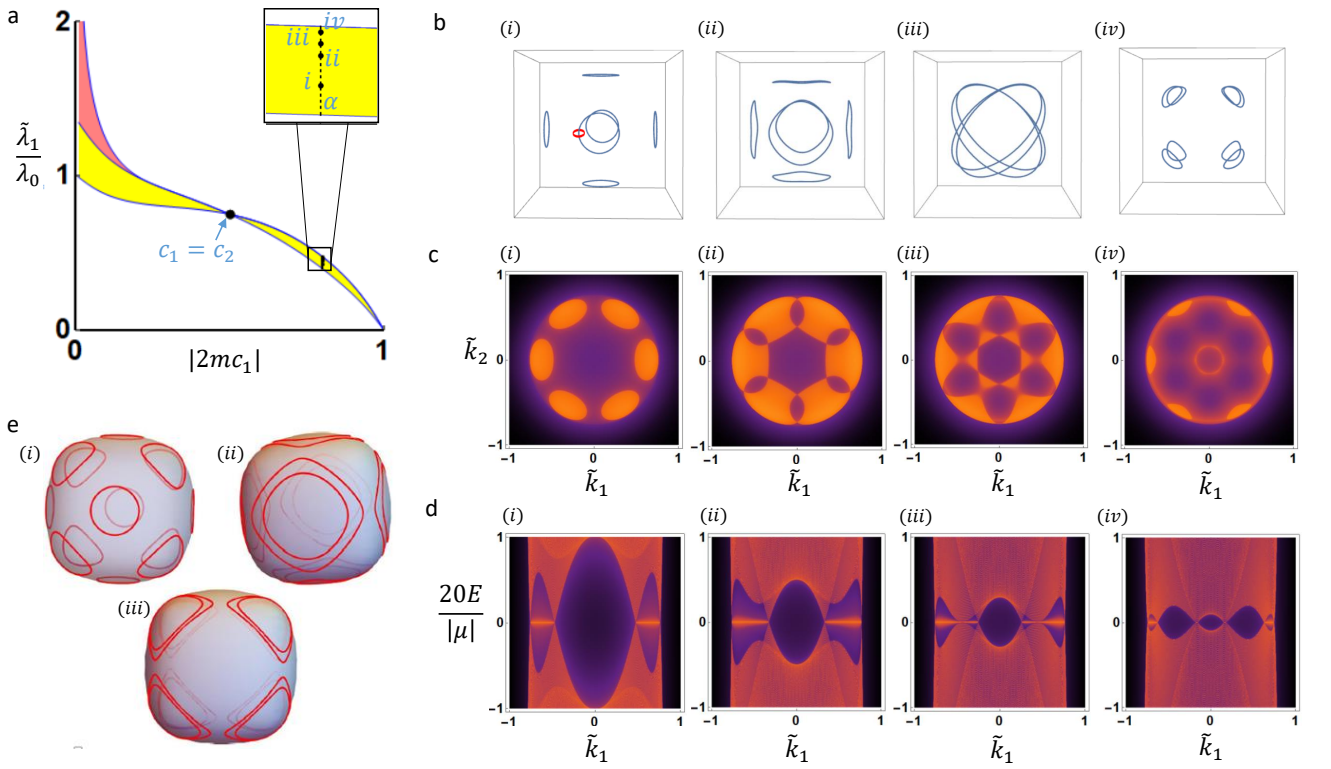

FIG. 2. (a) shows the phase diagram in the parameter space spanned by interaction strength ratio $\tilde{\lambda}_1/\lambda_0$ and symmetric SOC strength $|2mc_1|$. In the yellow and red regions, the system are nodal. In the inset, the dashed line indicates the path α ($2m|c_1| = -0.8$) with four points $i, ..., iv$ on it. Here $\tilde{\lambda}_1/\lambda_0 = 0.4246, 0.4507, 0.4615, 0.4716$ for (i), (ii), (iii), (iv), respectively. (b),(c) and (d) show the bulk nodal line structures (blue lines), zero-energy density of states on (111) surface and energy dispersion along $(11\bar{2})$ axis on (111) surface for the four points $i, ..., iv$ in the inset of (a). The red circle in (i) of (b) shows a typical path along which the topological invariant is calculated. $\tilde{k}_{1,2} = k_{1,2}/\sqrt{2m\mu}$ are momenta along $(11\bar{2})$ and $(\bar{1}10)$, respectively, and $c_1 > 0$ and $\tilde{\Delta}_0/|\mu| = 1$ are chosen. (e) shows three typical nodal structures in the red region of (a). Parameters are chosen as $2m|c_1| = -0.12$, $2m|c_2| = -0.5$ and $\tilde{\lambda}_1/\lambda_0 = 1.12$ for (i), $2m|c_1| = -0.12$, $2m|c_2| = -0.5$ and $\tilde{\lambda}_1/\lambda_0 = 1.155$ for (ii), and $2m|c_1| = -0.08$, $2m|c_2| = -0.5$ and $\tilde{\lambda}_1/\lambda_0 = 1.329$ for (iii).

and subdominant s-wave singlet pairing due to anti-symmetric SOC. Our theory provides a new explanation of the nodal structure as a result of singlet-quintet mixing induced by symmetric SOC. In half-Heusler compounds, symmetric SOC at the Fermi surface is similar to chemical potential ($\sim 20meV$), and much larger than that of anti-symmetric SOC ($\sim 4meV$)[14,22]. Thus, the contribution of the anti-symmetric SOC to the linearized gap equation is negligible, and its influence is to split one $N_w = \pm 2$ nodal line into two $N_w = \pm 1$ nodal lines[35]. In addition, the interaction in s-wave singlet channel is normally dominant for superconductivity in weakly correlated materials. Therefore, we expect singlet-quintet mixing should be dominant over singlet-septet mixing and response for nodal lines in half-Heusler SCs. We notice additional surface arcs existing around the Γ point for singlet-septet mixing (Fig.5a in Ref.[17]), but absent for singlet-quintet mixing (Fig.2c(ii)) due to its inversion-preserving nature[35]. Such qualitatively difference might be experimentally tested through scanning tunneling microscopy to distinguish two pairing-mixed states.

In conclusion, we theoretically propose a new singlet-quintet mixing in the Luttinger model, which leads to TNLS with surface flat Majorana bands. Such mechanism provides a new understanding of recent experiments in half-Heusler SCs[15]. Its distinct experimental signatures from other possible mechanisms are considered and can be tested in the future experiments. As mentioned above, due to the inversion-preserving nature of the singlet-quintet mixing, our work suggests a new direction of pairing mixing between different spin channels in not only non-centrosymmetric but also centrosymmetric SCs with high-spin electrons (e.g. Sr_3SnO). The TNLS and the corresponding surface Majorana band of half-Heusler SCs suggest a new platform for exploring topological superconductivity and topological quantum computation.

VI. Acknowledgement

JY thanks Lun-Hui Hu, Yang Ge, Rui-Xing Zhang and Jian-Xiao Zhang for helpful discussion. CXL and JY acknowledge the support from Office of Naval Research (Grant No. N00014-15-1-2675 and renewal No. N00014-18-1-2793).

* cxl56@psu.edu

[1] E. Bauer and M. Sigrist, *Non-centrosymmetric superconductors: introduction and overview*, Vol. 847 (Springer Science & Business Media, 2012).
[2] L. P. Gor'kov and E. I. Rashba, Phys. Rev. Lett. **87**, 037004 (2001).
[3] P. A. Frigeri, D. F. Agterberg, A. Koga, and M. Sigrist, Phys. Rev. Lett. **92**, 097001 (2004).
[4] T. Yasuda, H. Shishido, T. Ueda, S. Hashimoto, R. Settai, T. Takeuchi, T. D Matsuda, Y. Haga, and Y. Ōnuki, Journal of the Physical Society of Japan **73**, 1657 (2004).
[5] T. Takeuchi, T. Yasuda, M. Tsujino, H. Shishido, R. Settai, H. Harima, and Y. Ōnuki, Journal of the Physical Society of Japan **76**, 014702 (2006).
[6] R. Settai, Y. Miyauchi, T. Takeuchi, F. Lévy, I. Sheikin, and Y. Ōnuki, Journal of the Physical Society of Japan **77**, 073705 (2008).
[7] H. Mukuda, T. Ohara, M. Yashima, Y. Kitaoka, R. Settai, Y. Ōnuki, K. Itoh, and E. Haller, Physical review letters **104**, 017002 (2010).
[8] S. K. Yip, Phys. Rev. B **65**, 144508 (2002).
[9] V. M. Edelstein, Phys. Rev. Lett. **75**, 2004 (1995).
[10] S. Fujimoto, Phys. Rev. B **72**, 024515 (2005).
[11] M. Sato and S. Fujimoto, Phys. Rev. B **79**, 094504 (2009).
[12] Y. Tanaka, T. Yokoyama, A. V. Balatsky, and N. Nagaosa, Phys. Rev. B **79**, 060505 (2009).
[13] T. Yoshida, A. Daido, Y. Yanase, and N. Kawakami, Phys. Rev. Lett. **118**, 147001 (2017).
[14] P. M. R. Brydon, L. Wang, M. Weinert, and D. F. Agterberg, Phys. Rev. Lett. **116**, 177001 (2016).
[15] H. Kim, K. Wang, Y. Nakajima, R. Hu, S. Ziemak, P. Syers, L. Wang, H. Hodovanets, J. D. Denlinger, P. M. R. Brydon, D. F. Agterberg, M. A. Tanatar, R. Prozorov, and J. Paglione, Science Advances **4** (2018), 10.1126/sciadv.aao4513.
[16] W. Yang, T. Xiang, and C. Wu, Phys. Rev. B **96**, 144514 (2017).
[17] C. Timm, A. P. Schnyder, D. F. Agterberg, and P. M. R. Brydon, Phys. Rev. B **96**, 094526 (2017).
[18] B. Roy, S. A. A. Ghorashi, M. S. Foster, and A. H. Nevidomskyy, arXiv preprint arXiv:1708.07825 (2017).
[19] I. Boettcher and I. F. Herbut, Phys. Rev. Lett. **120**, 057002 (2018).
[20] W. Yang, Y. Li, and C. Wu, Phys. Rev. Lett. **117**, 075301 (2016).
[21] J. W. F. Venderbos, L. Savary, J. Ruhman, P. A. Lee, and L. Fu, Phys. Rev. X **8**, 011029 (2018).
[22] L. Savary, J. Ruhman, J. W. F. Venderbos, L. Fu, and P. A. Lee, Phys. Rev. B **96**, 214514 (2017).
[23] S. A. A. Ghorashi, S. Davis, and M. S. Foster, Phys. Rev. B **95**, 144503 (2017).
[24] N. P. Butch, P. Syers, K. Kirshenbaum, A. P. Hope, and J. Paglione, Phys. Rev. B **84**, 220504 (2011).
[25] T. V. Bay, T. Naka, Y. K. Huang, and A. de Visser, Phys. Rev. B **86**, 064515 (2012).
[26] M. Meinert, Phys. Rev. Lett. **116**, 137001 (2016).
[27] M. Oudah, A. Ikeda, J. N. Hausmann, S. Yonezawa, T. Fukumoto, S. Kobayashi, M. Sato, and Y. Maeno, Nature communications **7**, 13617 (2016).
[28] J. Hausmann, M. Oudah, A. Ikeda, S. Yonezawa, and Y. Maeno, Superconductor Science and Technology **31**, 055012 (2018).
[29] A. Ikeda, T. Fukumoto, M. Oudah, J. N. Hausmann, S. Yonezawa, S. Kobayashi, M. Sato, C. Tassel, F. Takeiri, H. Takatsu, H. Kageyama, and Y. Maeno, Physica B: Condensed Matter **536**, 752 (2018).
[30] T. Kawakami, T. Okamura, S. Kobayashi, and M. Sato, arXiv preprint arXiv:1802.09962 (2018).
[31] C. Wu, Modern Physics Letters B **20**, 1707 (2006).
[32] R. Winkler, S. Papadakis, E. De Poortere, and M. Shayegan, *Spin-Orbit Coupling in Two-Dimensional Electron and Hole Systems*, Vol. 41 (Springer, 2003) pp. 211–223.
[33] S. Chadov, X. Qi, J. Kübler, G. H. Fecher, C. Felser, and S. C. Zhang, Nature materials **9**, 541 (2010).
[34] J. M. Luttinger, Phys. Rev. **102**, 1030 (1956).
[35] See Supplementary Material [url] for details of conventions, the linearized gap equation and topological nodal-line superconductivity, which includes Ref.[36–40].
[36] S. Murakami, N. Nagosa, and S.-C. Zhang, Phys. Rev. B **69**, 235206 (2004).
[37] P. A. Frigeri, D. F. Agterberg, A. Koga, and M. Sigrist, Phys. Rev. Lett. **92**, 097001 (2004).
[38] X.-L. Qi, T. L. Hughes, and S.-C. Zhang, Phys. Rev. B **81**, 134508 (2010).
[39] G.-m. Zhao, Phys. Rev. B **64**, 024503 (2001).
[40] B. H. Brandow, Phys. Rev. B **65**, 054503 (2002).
[41] G. Dresselhaus, Phys. Rev. **100**, 580 (1955).
[42] E. O. Kane, Journal of Physics and Chemistry of Solids **1**, 249 (1957).
[43] H. Yang, J. Yu, S. S. P. Parkin, C. Felser, C.-X. Liu, and B. Yan, Phys. Rev. Lett. **119**, 136401 (2017).
[44] A. P. Schnyder, P. M. R. Brydon, and C. Timm, Phys. Rev. B **85**, 024522 (2012).
[45] P. M. R. Brydon, A. P. Schnyder, and C. Timm, Phys. Rev. B **84**, 020501 (2011).
[46] K. Yada, M. Sato, Y. Tanaka, and T. Yokoyama, Phys. Rev. B **83**, 064505 (2011).
[47] A. P. Schnyder and S. Ryu, Phys. Rev. B **84**, 060504 (2011).
[48] A. A. Burkov, M. D. Hook, and L. Balents, Phys. Rev. B **84**, 235126 (2011).

[49] C. Fang, Y. Chen, H.-Y. Kee, and L. Fu, Phys. Rev. B **92**, 081201 (2015).
[50] M. L. Sancho, J. L. Sancho, J. L. Sancho, and J. Rubio, Journal of Physics F: Metal Physics **15**, 851 (1985).
[51] Y. Nakajima, R. Hu, K. Kirshenbaum, A. Hughes, P. Syers, X. Wang, K. Wang, R. Wang, S. R. Saha, D. Pratt, *et al.*, Science advances **1**, e1500242 (2015).